International Journal of Greenhouse Gas Control 94 (2020) 102929

Contents lists available at ScienceDirect

International Journal of Greenhouse Gas Control

journal homepage: www.elsevier.com/locate/ijggc

A study of designer amine 4-amino-1-propyl-piperidine against the corrosion of carbon steel for application in CO_2 capture

Xiaoqin Li[a,b], Pauline Pearson[c], Qi Yang[b,*], Graeme Puxty[d], Paul Feron[d], Dan Xiao[a,*]

[a] Institute of New Energy and Low-Carbon Technology, Sichuan University, Chengdu, PR China
[b] CSIRO Manufacturing, Research Way, Clayton, Vic, 3168, Australia
[c] CSIRO Energy, Research Way, Clayton, Vic, 3168, Australia
[d] CSIRO Energy, 10 Murray Dwyer Circuit, Mayfield West, NSW, 2304, Australia

ARTICLE INFO

Keywords:
Carbon steel
4-Amino-1-propyl-piperidine
Electrochemical corrosion
Hydrothermal corrosion
$FeCO_3$
CO_2 capture

ABSTRACT

We investigated the relationship between amine structure and corrosion rates in a study of the corrosion behaviour of carbon steel in CO_2-loaded 4-amino-1-propyl-piperidine (4A1PPD) solution and a series of related amines. Electrochemical measurements showed that 4A1PPD displayed the lowest corrosion rate of the amines studied, and that the corrosion rate decreased with the increase of the number of substituents on amino groups and a structural change from linear amines to cyclic amines. We also carried out a hydrothermal corrosion study using selected amines to analyse the surface morphology and composition formed on the surface of corroded carbon steel. The results suggested that the formation of a protective film was dependant on the ratio of bicarbonate/carbamate species. We confirmed that a dense $FeCO_3$ protective film was produced on the carbon steel surface after hydrothermal corrosion treatment with CO_2 rich 4A1PPD solution. Our results demonstrate that the 4A1PPD designer amine with a cyclic structure shows good corrosion properties for use in post-combustion CO_2 capture and resulted in significantly reduced corrosion on carbon steel compared to the benchmark amine, monoethanolamine.

1. Introduction

The most commonly used absorbents for post-combustion capture of CO_2 (PCC) are aqueous alkanolamine solutions (Conway et al., 2015a,b; Conway et al., 2013). Unfortunately, aqueous amine absorbents can corrode equipment, which is one of the major issues facing CO_2 capture technologies. Although amines can actually inhibit some corrosion processes (Garcia-Arriaga et al., 2010), under CO_2 capture conditions they are able to cause severe corrosion to carbon steel equipment due to the formation of bicarbonate and carbamate species (Gao et al., 2012; Soosaiprakasam and Veawab, 2008; Zheng et al., 2015). Some strategies, such as the application of a protective film coating (Nešić and Lee, 2003), the addition of corrosion inhibitors to the amine solutions (Sığırcık et al., 2016), the use of corrosion-resistant materials (Billingham et al., 2011) and the implementation of alternative absorption liquids (Zheng et al., 2014), have been applied to reduce corrosion in PCC plant. Among these methods, alternative amine based absorption liquids are considered particularly effective in reducing corrosion in process equipment used for CO_2 capture due to the self-formation of a protective film in the CO_2-loaded amine solution. Solutions with a high concentration of bicarbonate and low concentration of carbamate favour the formation of an effective protective film, but this protective film can be damaged by a solution with high concentration of carbamate (Nielsen, 1997). Therefore, it is necessary to design an amine with suitable speciation (carbamate and bicarbonate) to reduce corrosivity under typical PCC operating conditions.

The combined corrosion effects of CO_2 and impurity (e.g SO_2, O_2, NO_X et al) have been studied. (Kladkaew et al., 2009; Krzemień et al., 2016) Due to the complicated mechanism of corrosion in these mixed systems, our current work focuses on the impact of amine structural feature change on their corrosion performance on the surface of CS1018 carbon steel in the presence of CO_2. Hence, flue gas impurities which may affect the corrosion process are not investigated in this work.

The corrosion mechanism at the interface between CO_2-loaded amine solutions and a steel surface has been widely reported (Veawab and Aroonwilas, 2002; Zheng et al., 2015; Zheng et al., 2014, 2016c). The consumption of both Fe^{2+} and electrons can promote Fe dissolution via the anodic reaction (1),

Anodic reaction:

$$Fe \leftrightarrow Fe^{2+} + 2e^{-} \quad (1)$$

* Corresponding authors.
E-mail address: xiaodan@scu.edu.cn (D. Xiao).

https://doi.org/10.1016/j.ijggc.2019.102929
Received 3 March 2019; Received in revised form 1 October 2019; Accepted 27 November 2019

The electrochemical cathodic reactions are complicated (reactions 2–4), since a CO_2-loaded amine system can contain various species, such as hydrogen ions (H^+), carbonic acid (H_2CO_3), carbonate (CO_3^{2-}), bicarbonate (HCO_3-) and carbamate (AmCOO-). This system has a relatively high pH (< 8), resulting in the low concentrations of H^+ and H_2CO_3 and the cathodic reaction is mainly reaction (4).

Cathodic reactions:

$$2H^+ + 2e^- \leftrightarrow H_2 \quad (2)$$

$$2H_2CO_3 + 2e^- \leftrightarrow 2HCO_3^- + H_2 \quad (3)$$

$$2HCO_3^- + 2e^- \leftrightarrow 2CO_3^{2-} + H_2 \quad (4)$$

The Fe^{2+} ions can be consumed via the formation of precipitants (reactions 5–7). In addition, some stable precipitants have protective properties that inhibit further corrosion of carbon steel, e.g. $FeCO_3$ can form a film that acts as a physical barrier to restrict the contact of metal substrate with the solution (Sedransk Campbell et al., 2017; Sun and Nesic, 2006; Zheng et al., 2016b).

$$Fe^{2+} + CO_3^{2-} \rightarrow FeCO_3\downarrow \quad (5)$$

$$Fe^{2+} + OH^- \rightarrow Fe(OH)_2\downarrow \quad (6)$$

$$2Fe^{2+} + 2OH^- + CO_3^{2-} \rightarrow Fe_2CO_3(OH)_2\downarrow \quad (7)$$

Reaction (5) shows that the concentrations of both Fe^{2+} and CO_3^{2-} near the steel surface significantly affect the formation of $FeCO_3$. In CO_2-loaded amine solutions, the concentration of CO_3^{2-} is proportional to that of HCO_3- via reactions 8–11, where Am is an amine, AmCOO- is the carbamate form of the amine, and AmH^+ is the protonated amine (Zheng et al., 2016b). It has previously been reported that amines (Raeissi and Golozar, 2009), protonated amine ions (Nainar and Veawab, 2009) and carbamate ions (Tomoe et al., 1996) can promote corrosion by damaging the protective films. We therefore expect that the fast formation of carbonate ions is beneficial to the early formation of a protective $FeCO_3$ film on the metal surface, which can prevent corrosion at the initial stage.

$$CO_2\,(g) \leftrightarrow CO_2\,(aq) \quad (8)$$

$$2Am + CO_2 \leftrightarrow AmCOO^- + AmH^+ \quad (9)$$

$$AmCOO^- + H_2O \leftrightarrow Am + HCO_3^- \quad (10)$$

$$HCO_3^- + H_2O \leftrightarrow CO_3^{2-} + H_3O^+ \quad (11)$$

The amine structure plays an important role in speciation upon reaction with CO_2. Primary (1°) and secondary (2°) amines directly react with CO_2 to form carbamates, which play multiple roles in corrosion (Rochelle, 2012). Carbamates then hydrolyse to bicarbonate via reaction 10. The carbamate formation is very fast, while its hydrolysis is strongly affected by the amine's structure. The CO_2 capture mechanisms of tertiary (3°) and sterically hindered amines are different from that of 1° and 2° amines (reactions 12 and 13).

Sterically hindered amines:

$$\mathrm{R}-NH_2 + CO_2(aq) + H_2O \leftrightarrow \mathrm{R}-NH_3^+ + HCO_3^- \quad (12)$$

Tertiary amines:

$$R_1R_2R_3N + CO_2(aq) + H_2O \leftrightarrow R_1R_2R_3N^+H + HCO_3^- \quad (13)$$

In this pathway, the amines can directly form bicarbonate and carbonate species with a hydrolysed CO_2 product after CO_2 dissolution (Behrens et al., 2017). However, CO_2 absorption in solutions of sterically hindered amines or tertiary amines is slow. The effect of amine structures on CO_2 absorption behaviours has been explored in our previous work (Li et al., 2017; Xiao et al., 2019; Yang et al., 2016), but few studies concern the influence of amine structure on corrosion, especially the difference between linear and cyclic amines (Hatchell et al., 2015). Previous studies within our group have shown that diamines with space of C3 between two amino groups in a molecule demonstrate reasonable performance for CO_2 capture. Among these amines, the cyclic diamine 4-amino-1-propyl-piperidine (4A1PPD) exhibits the highest concentration of carbonate.(Xiao et al., 2019; Yang et al., 2016) Hence, 4A1PPD, with its parallel linear diamines, makes a good model to explore the influence of amine structures on the corrosion of carbon steel in CO_2 capture.

In this work, the corrosion of carbon steel was studied using CO_2-loaded 4A1PPD. Both electrochemical and hydrothermal corrosion methods were used to investigate corrosion rates and the factors affecting corrosion. Several related diamines were also studied to correlate amine structural changes, such as the number of substituents on the same amino group and the cyclic structure versus linear structure, with carbon steel corrosion. Monoethanolamine (MEA) was tested under the same condition as a benchmark to evaluate the performance of the studied diamines.

2. Experimental

2.1. Electrochemical testing

2.1.1. Solution preparation and analysis

All of the amines were used as supplied: MEA (≥99 %, Merck), 1.3-diaminopropane (1,3-DAP, ≥98 %, Alfa Aesar), 3-(methylamino)propylamine (3MAPA, ≥97 %, Fluka), 3-(dimethylamino)-1-propylamine (3DMA1PA, ≥99 %, Alfa Aesar), piperidin-4-amine (4APD, ≥98 %, Combi-Blocks) and 4A1PPD (≥99 %, prepared in-house) (Yang et al., 2016). The amines were diluted to the desired concentration using deionised water. The benchmark solution for CO_2 capture applications is 5 M (~30 wt%) MEA. As each mole of diamine has the doubled amino-functionality as that of MEA, the concentration of ~2.5 M was chosen for all diamines in this study to allow a fair comparison with 5 M MEA. The electrochemical corrosion tests were performed in CO_2-loadedamine solutions: 150 mL of each solution was loaded with CO_2 (BOC Australia, industrial grade, > 99.9 %), flow rate 12.5 mL/min, for 24 h at room temperature and at atmospheric pressure. The concentration of amine and CO_2 loading were verified by quantitative ^{13}C NMR spectroscopy (Li et al., 2018), as shown in Table 1.

2.1.2. Preparation of working electrode

The diameter and thickness of the working electrode (CS1018) was 15 mm and 2 mm respectively. The chemical composition of CS1018 working electrodes were 0.15–0.20 wt% C, 0.60–0.90 wt% Mn, max0.04 wt% P, max0.05 wt% S and balance Fe. Immediately prior to contact with the test solution, the CS1018 working electrodes were wet-polished with different grades of sandpaper (200 and 600 grit Si/C paper, in turn). The polished CS1018 electrodes were mounted in a Teflon sample holder after rinsing several times with distilled water. The surface area of CS1018 exposed to test amine solutions was 0.785

Table 1
The details of amines used in this work, including the amine structure, the concentration of amine (C_{amine}), the CO_2 loading and the concentration of CO_2 (C_{CO2}).

Amine	Structure	C_{amine} (M)	CO_2 loading (mol CO_2/mol amine)	C_{CO2} (M)
MEA		5	0.735	3.68
1,3-DAP		2.5	1.383	3.46
3MAPA		2.5	1.418	3.55
3DMA1PA		2.5	1.417	3.54
4APD		2.5	1.553	3.88
4A1PPD		2.5	1.591	3.98

cm^2.

2.1.3. Experimental setup and procedures

The experimental setup was the same as previously reported (Pearson et al., 2013), which consisted of a cell, a gas supply and a potentiostat (Ecochemie Autolab PGSTAT302 N) connected to a PC running NOVA version 1.11 software for experimental control and analysis. The glass cell, supplied by Ecochemie Autolab, had a 400 mL capacity and was equipped with several ports for solution entrance, gas inlet–outlet and electrodes. A carbon steel disc (CS1018), Ag/AgCl and two 316 stainless steel rods were used as working, reference and counter electrodes, respectively. The Ag/AgCl electrode was placed inside a Luggin capillary and filled with KCl solution (3 M). The counter electrode was 2 mm in diameter. A stirrer was also used as required.

The amine solutions were degassed with nitrogen for at least 60 min before being contacted with the working electrode. The open circuit potential (OCP) of the cells was measured until they were stable (defined as $\Delta OCP < 5$ mV/10 min). The linear polarization resistance (LPR) method, with a scan rate of 0.167 mV/s and potential range from −20 mV to +20 mV vs. OCP, was applied to estimate the polarization resistance (R_p). Electrochemical impedance spectroscopy (EIS) scans were performed over the frequency range from 10 kHz to 4 mHz. The number of frequencies was 70 with logarithmic distribution, and the applied DC potential was OCP, with an amplitude of 10 mV. Tafel plots were measured at a scan rate of 0.167 mV/s with the potential ranging from –250 to +250 mV vs. OCP. All tests were conducted at 40 °C and each test was measured at least twice on a fresh batch of solvent/fresh working electrode. Before and after each electrochemical test, the OCP was measured until the readings were stable to monitor the stability of the electrode. After electrochemical corrosion testing, the corroded CS1018 samples were quickly rinsed with deionised water and absolute ethanol in sequence, and then dried with N_2 gas. The samples were stored under N_2 atmosphere until surface analysis was performed.

The corrosion rates were calculated from Tafel curves using the built-in 'corrosion rate, fit' analysis in the NOVA version 1.11 software. This fits data to the Butler–Volmer equation to find the corrosion current, i_{corr} (A). The corrosion rate can be calculated using:

$$CR = \frac{K \bullet i_{corr} \bullet EW}{A \bullet \rho} \quad (14)$$

where K is a constant (3272 mm/(amp • cm • year)), and EW, A and ρ are the equivalent weight (g) of specimen, area of working electrode (cm^2) and density of specimen (g cm^{-3}), respectively.

2.2. Hydrothermal corrosion treatment

MEA, 3DMA1PA and 4A1PPD solutions (25 mL) with the same concentrations as in Section 2.1.1 were loaded with pure CO_2 at flow rate of 12.5 mL min^{-1} for 6 h at room temperature. Then, the CO_2-loaded amine solutions (4 mL) were added into a 10 mL Teflon autoclave and a polished CS1018 specimen (as described in Section 2.1.2) was immersed in this solution. To inhibit the influence of oxygen, all processes were conducted under N_2. Duplicate samples of each CO_2-loaded solution were prepared. Hydrothermal corrosion was carried out for nine days at 80 °C. The species of CO_2-loaded amines were also determined by quantitative ^{13}C NMR spectroscopy. After corrosion, the carbon steel disc samples were washed and stored as described in Section 2.1.3.

For the mass loss (M, mg) calculation, the carbon steel specimen were chemically cleaned to remove the corrosion product according to the ASTM G1-90 standard (Formula C.3.5).(ASTM G1, 1999) The corroded disc was immersed in 5 ml of the solution and soaked for 30 min. The disc was then removed from the cleaning solution and rinsed with DI water, methanol, dried with N_2 gas blowing, and weighed. The cleaning solution is a 1000 mL solution containing 530 mL of hydrochloric acid (HCl, specific gravity 1.16) and 3.5 *g* of hexamethylene tetramine. The mass loss reflects corrosion performance of each solvent as the tested discs have similar exposed surface area. The M was calculated using the following equation

$$M = m_0 - m_1 \quad (15)$$

where m_0 and m_1 are the mass before corrosion (mg) and mass after removal of corrosion product (mg).

2.3. Characterization

The surface morphology of CS1018 after all the electrochemical tests was measured by scanning electron microscopy (SEM, ZEISS Gemini 2, Germany) and the corresponding surface element contributions were characterised by energy dispersive spectroscopy (EDS) and EDS mapping images. Quantitative carbon (^{13}C) NMR spectra were collected on a Bruker Avance Ascend III 400 NMR spectrometer at 25 °C to analyse the chemical compositions in the amine solution before and after CO_2 loading (Li et al., 2018).

After hydrothermal treatment, the surface morphologies of CS1018 discs and the corresponding surface element contributions were also measured. The concentration of Fe ions in the solution was measured by Varian 730-ES axial inductively coupled plasma optical emissions spectroscopy (ICP-OES). The crystalline structures of compounds on the CS1018 surface before and after corrosion in CO_2-loaded amine solutions were determined directly by X-ray diffraction (XRD). For the freshly polished CS1018, MEA and 4A1PPD treated metal coupons, data was collected with a Rigaku SmartLab x-ray diffractometer, equipped with a rotating anode CuK_α source (45 kV, 200 mA) and a Hypix 3000 detector, operated in grazing incidence mode to enhance the diffracted signal compared with the surface phases. The data were collected from the 3DMA1PA treated metal coupon with a Bruker D8 Advance x-ray diffractometer operating under CoKα radiation (35 kV, 45 mA) equipped with a Lynx Eye detector, as this sample fluoresced under the incident CuK_α beam available on the grazing incidence machine. The surface composition of corroded CS1018 was further analysed by X-ray photo spectroscopy (XPS, Kratos Analytical Inc AXIS Ultra-DLD, U.K.).

3. Results and discussion

3.1. Electrochemical corrosion behaviour

The LPR results provide a clear understanding of the impact of amine structure changes on the corrosivity of amines in CO_2 capture, as shown in Fig. 1a. The slope of the LPR curve is proportional to the resistance polarisation, R_p, which is inversely proportional to the corrosion rate; that is, a lower slope of the LPR curve indicates a lower corrosion rate, and a steeper slope demonstrates a higher corrosion rate. 1,3-DAP, showed the lowest R_p value (Fig. 1b), which corresponds to the highest corrosivity among the amines in this study. With the increase of methyl substituents on one amino group, an increasing R_p was observed from 1,3-DAP, 3MAPA to 3-DMPA. Comparing R_p values between 3MAPA and 4APD and/or between 3DMA1PA and 4A1PPD linked the change from linear to cyclic features in the amine molecules to decreasing corrosivity.

The R_p values of tested CO_2-loaded diamines can be ranked as 1,3-DAP < 3MAPA < 3DMA1PA, 3MAPA < 4APD ≈ 3DMA1PA < 4A1PPD. These results demonstrate that more methyl substituents and a cyclic moiety increase the R_p values of CO_2-loaded diamine solution, and hence reduce the corresponding corrosion rate of carbon steel in the respective solution. The designer amine 4A1PPD, in particular, showed the largest R_p value in comparison with its parallel linear diamine (3DMA1PA) and the similar cyclic diamine with fewer alkyl substituents (4APD). The electrochemical results presented in the following sections further support these results.

EIS measurements were conducted to further investigate the corrosion behaviour of CS1018 in CO_2-loaded amine solutions and the

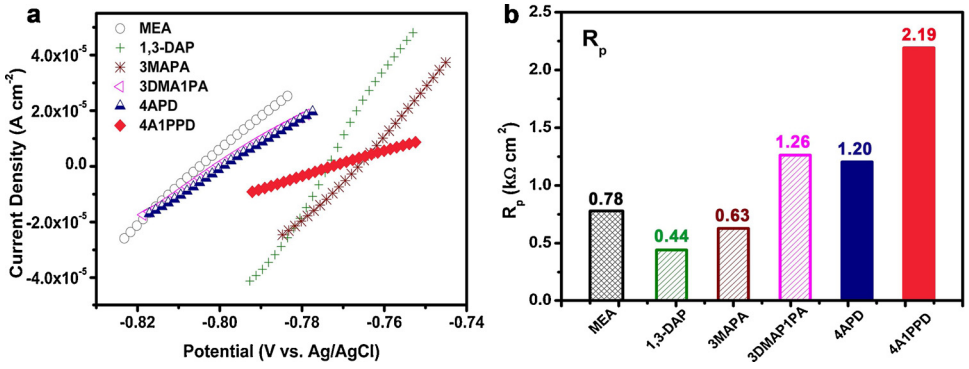

Fig. 1. (a) The LPR plots of MEA, 1,3-DAP, 3MAPA, 3DMA1PA, 4APD and 4A1PPD, and (b) the R_p values of the tested amines from LPR.

electrochemical behaviour of the metal/solution interface, as shown in Fig. 2. All of the Nyquist plots (Fig. 2a) display a single capacitive loop with no diffusion limitations. This implies that corrosion of CS1018 in different CO_2-loaded amine solutions is mainly controlled by the charge transfer process (Sığırcık et al., 2016; Tang et al., 2010). Moreover, these plots do not display a perfect semicircle due to the non-ideal capacitive behaviours (Lebrini et al., 2007) which can be explained by the structure of the electrical double layer. Considering these, an electrochemical equivalent circuit used to simulate the impedance data is shown in the inset image of Fig. 2a. In this equivalent circuit, R_s is the solution resistance; it can be graphically determined from the real (X) axis intercept at high frequency in the Nyquist plots. All of the solutions showed high conductivity, as indicated by the low value of R_s. R_p, including charge transfer resistance and diffuse layer resistance (film resistance), can be directly determined from the diameter of semicircle of Nyquist plots. The value of R_p increased with the increase of the number of substituents and the structural change from linear amine to cyclic amine (Fig. 2a). To improve the fitting, the double layer capacitance (C_{dl}) is often replaced by a constant phase element (*CPE*) to explain the deviation from ideal capacitive behaviour because of surface roughness, heterogeneity and adsorption effects (Sun et al., 2012).

The values of *Rp*, *Rs* and *CPE* are presented in Table 2. The *Rp* of 1,3-DAP diamine was the lowest (0.56 kΩ cm^2) and that of the designer diamine 4A1PPD the highest (2.97 kΩ cm^2), which was in agreement with the trend from the LPR data. The increase of R_p may be caused by the formation of a protective layer that forms a barrier to corrosive media, a phenomenon that has been studied previously (Li et al., 2011). In addition, the *CPE* values change irregularly with the change of amine features from MEA to 4A1PPD. The lowest *CPE* was achieved in CO_2-loaded 4A1PPD solution, suggesting that the 4A1PPD amine molecules or the speciation after CO_2 loading can adsorb at the metal/solution interface to form a protective film on the steel surface, and then decrease the extent of dissolution reaction. This is an efficient way to promote the formation of a protective film.

The obtained Bode plots of CS1018 in different CO_2-loaded amine solutions are given in Fig. 2b and c. Fig. 2b shows that only one time constant was observed in these plots in a wide range of frequencies from 100 kHz to 0.1 Hz, suggesting a similar corrosion mechanism in all solutions. An increase of absolute impedance at low frequencies in Bode modulus plots (Fig. 2c) was seen with the change of amine structures: substituent number increase and change from linear to cyclic amines. The higher impedance correlates to the higher protection of the carbon steel against corrosion. The same trend is also detected in the shift of break-point frequency (*BPF*) to lower values with the amine structure changes (Table 3).

The values of *BPF* can be obtained from the slope of log *f* vs log |*Z*| curves based on the intersection of horizontal lines at low frequencies with the central straight line at middle frequencies. The shift of BPF is directly related to increased adsorption of products (e.g. protonated amines or the Fe-based precipitate) at the interface of CS1018/solution (Sığırcık et al., 2016). A lower *BPF* was observed (Table 3) due to the non-ideal capacitive behaviour between the metal/solution interface mentioned above. The results demonstrate that the solution with the 4A1PPD designer diamine is most effective in protecting against corrosion of CS1018.

The corrosion behaviour of CS1018 in CO_2-loaded amines was further investigation by the measurement of the polarization curves as shown in Fig. 3. No clear relationship between corrosion potential (E_{corr}) and amine structures could be determined. Noticeably, the anodic and cathodic current densities decreased with the increase of number of substituted methyl groups (1,3-DAP > 3MAPA > 3 DMA1PA) and the structural change from linear to cyclic feature (3MAPA vs. 4APD and 3DMA1PA vs. 4A1PPD). This suggests that both anodic and cathodic reactions were impeded by the reactants' transport rate to the surface of the working electrode (Emori et al., 2017). These results may be ascribed to the formation of protective film over the corroded surface. The electrochemical corrosion kinetic parameters (i.e., the anodic (β_a) and cathodic ($-\beta_c$) Tafel slopes, E_{corr}, corrosion current density (j_{corr}), R_p and corrosion rate) obtained from the Tafel polarization curves are summarized in Table 2. The value of j_{corr} decreased and that of R_p increased with the increase of numbers of substituents, and with the change of structure from linear to cyclic, as described for LPR and EIS.

We measured the surface morphologies and elemental analysis of the corroded CS1018 obtained from CO_2-loaded MEA and 4A1PPD solutions after electrochemical measurement to show the protective film on the carbon steel disc after electrochemical corrosion tests by SEM (Fig. 4), EDS and EDS elemental mapping (Fig. 5). The SEM images of the sample corroded in MEA solution showed a significantly rough surface (Fig. 4a) and the growth of some nanosheets on CS1018 (Fig. 4b). In contrast, the SEM image of CS1018 corroded in 4A1PPD solution displayed a smoother surface with few cracks or cavitations (Fig. 4c). Under high magnification (Fig. 4d), it is apparent that the scale formed was dense, and would be expected to provide better protection against corrosion than the loosely packed nanosheets observed in the MEA sample.

EDS and EDS mapping images were carried out to further investigate the composition of the protective film. Fe, C and O elements were detected for both of the samples corroded in CO_2-loaded MEA and 4A1PPD solutions (Fig. 5a and 5b). Carbon and oxygen levels were very low (C 5.0 wt%, O 1.2 wt% for MEA and C 4.8 wt%, O 0.9 wt% for 4A1PPD). Comparing the EDS mapping images of these two samples (from Fig. 5c to 5j), the elemental distribution of Fe, C and O was evenly distributed on the sample exposed to 4A1PPD solution, but carbon and oxygen were concentrated on some points for the sample obtained from MEA solution. These results verify that a protective film is formed on the surface of CS1018 after corrosion tests in the 4A1PPD solution, implying that the designer amine 4A1PPD with cyclic structure has the potential to reduce metal corrosion in CO_2 capture plant.

Quantitative ^{13}C NMR spectroscopy was used to investigate the

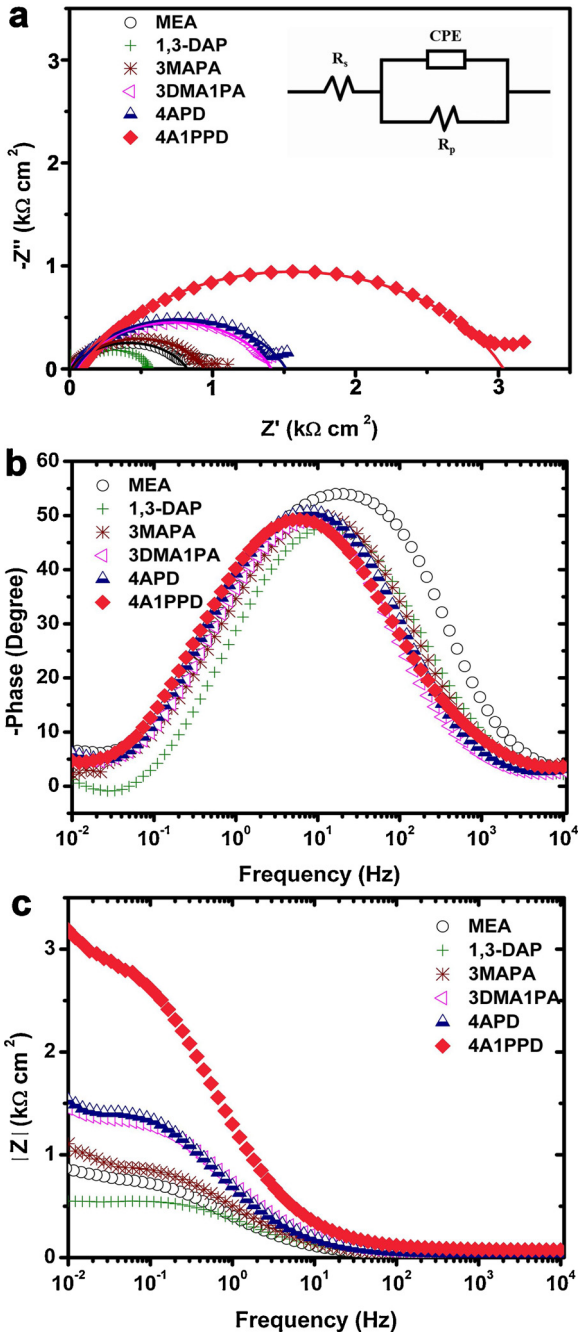

Fig. 2. (a) Nyquist plots, the inset image is the equivalent electrical circuit (simplified Randles circuit) used to identify and fit the EIS plots, (b) Bode phase and (c) Bode modulus plots of MEA, 1,3-DAP, 3MAPA, 3DMA1PA, 4APD and 4A1PPD.

Table 3
The break-point frequency (BPF) in Fig. 2c for CO_2-loaded MEA, 1,3-DAP, 3MAPA, 3DMA1PA, 4APD and 4A1PPD.

	MEA	1,3-DAP	3MAPA	3DMA1PA	4APD	4A1PPD
BPF (Hz)	12.80	18.89	11.64	8.76	7.57	6.56

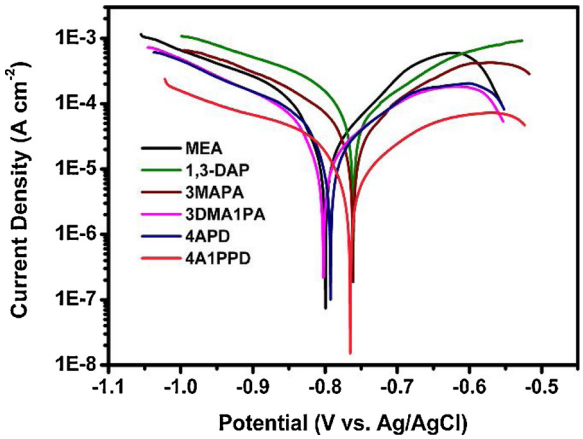

Fig. 3. Polarization curves of MEA, 1,3-DAP, 3MAPA, 3DMA1PA, 4APD and 4A1PPD.

concentrations of bicarbonate and carbamate in each amine solution after the solution was loaded with CO_2. The ^{13}C NMR spectra of 4A1PPD before and after CO_2 loading are displayed in Fig. 6 to illustrate the species formed in the system. Two new peaks appeared at low magnetic field: carbamate (S_2) and bicarbonate (S_1) after CO_2 absorption, and the signals of aliphatic carbons were observed shifting towards higher magnetic field due to the falling solution pH values during CO_2 loading.

Previous studies have shown that a protective film is more likely to form on the surface of steel in amine solutions with a high concentration of bicarbonate, and that these films may be damaged in high concentration of carbamate because the amine carbamate can complex ferrous/ferric ions (Guo and Tomoe, 1998; Tomoe et al., 1996). As shown in Table 4, the CO_2-loaded 1,3-DAP solution had the lowest concentration of bicarbonate and the highest concentration of carbamate. This is consistent with CS1018 displaying the worst corrosion behaviour in 1,3-DAP solution.

Correlating the speciation to amine structures, the concentration of carbamate decreased and that of bicarbonate increased with more methyl substituents. The CO_2-loaded cyclic amines (4APD and 4A1PPD) exhibited higher bicarbonate and lower carbamate concentration than their comparable linear amines (3MAPA and 4DMA1PA). The cyclic designer diamine (4A1PPD) reached the highest bicarbonate concentration. This high bicarbonate concentration promotes a faster formation of $FeCO_3$ protective film on the carbon steel surface. Typically greater CO_2 leads to higher corrosion rates. However, the lowest

Table 2
Electrochemical parameters fitted from electrochemical impedance spectroscopy (EIS) and the polarization curve.

AMINE	EIS			Polarization curves					
	R_p (kΩ cm^2)	R_s (kΩ cm^2, ×10^{-3})	*CPE* (uF cm^{-2})	β_a (V dec^{-1})	$-\beta_c$ (V dec^{-1})	E_{corr} (V)	j_{corr} (uA cm^{-2})	R_p (kΩ cm^2)	Corrosion rate (mm year^{-1})
MEA	0.82	10.10	502.66	0.08	0.11	−0.80	45.91	0.69	0.53
1.3DAP	0.56	18.50	377.87	0.38	0.40	−0.76	350.28	0.39	4.06
3MAPA	0.94	24.65	382.59	0.08	0.13	−0.76	46.96	0.77	0.54
3DMA1PA	1.38	47.39	288.38	0.11	0.21	−0.80	39.89	1.31	0.46
4APD	1.48	38.31	332.17	0.11	0.16	−0.79	36.25	1.27	0.42
4A1PPD	2.97	71.60	192.47	0.13	0.26	−0.77	19.69	3.04	0.23

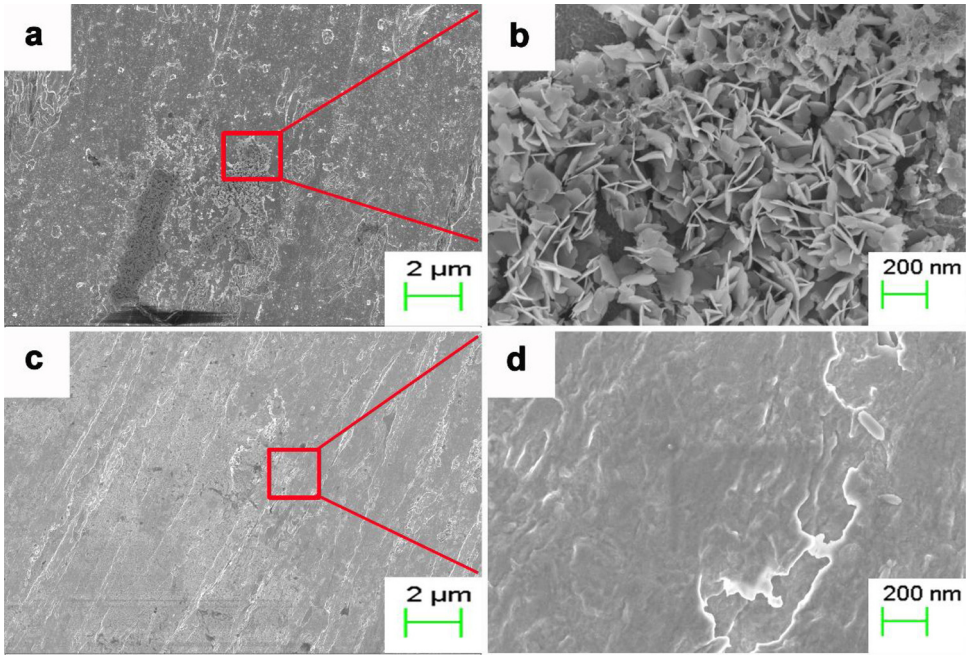

Fig. 4. Scanning electron microscope (SEM) images of corroded CS1018 in CO_2-loaded MEA (a, b) and 4A1PPD (c, d) after electrochemical measurements.

corrosion rate on the carbon steel was observed in the CO_2 loaded 4A1PPD solution even though this amine had the highest CO_2 loading among all the amines in this study. This adds another advantage to 4A1PPD as an excellent CO_2-capture solution in addition to its lower regeneration energy requirement than other five studied amines.

3.2. Hydrothermal treatment

Next we investigated the corrosion behaviour of CS1018 in a CO_2-loaded designer amine 4A1PPD solution, by a hydrothermal treatment method. MEA, which is the benchmark amine in PCC, was also investigated under the same experimental conditions, along with 3DMA1PA, the best linear amine tested. The CO_2 loaded amine solutions were prepared in a shorter absorption time as only 25 ml of amine solutions were used to make the rich stock solutions. The initially reflective surface of CS1018 was coated by a dark-grey film after hydrothermal treatment in MEA, 3DMA1PA and 4A1PPD solutions for nine days (Table 5).

The CS1018 disc exposed to MEA solution had the highest mass loss (12.73 mg) (Table 5) whilst the disc treated with 4A1PPD shows the lowest mass loss (3.17 mg) in this test, which is in agreement with corrosion results from the electrochemical study. The solution concentrations of Fe after hydrothermal corrosion were determined by ICP-OES, and were much lower in the 4A1PPD solution (0.89 ppm Fe) and 3DMA1PD solution (0.13 ppm Fe), than in the MEA solution (39.00 ppm Fe) solution. The minor difference of Fe concentrations between 4A1PPD and 3DMA1PD solutions is within the experimental variation. The Fe concentration results are consistent with the mass loss observed on the disc in MEA, ie dissolution of iron, and weight gain in 4A1PPD and 3DMA1PD, ie any dissolved iron was rapidly precipitated

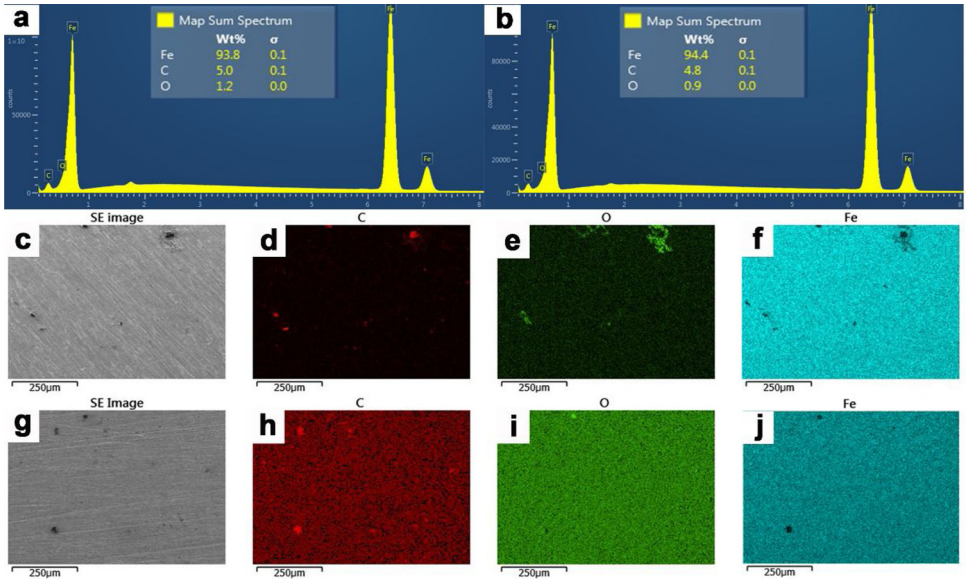

Fig. 5. Energy dispersive spectroscopy (EDS) measurements of CS1018 corroded in CO_2-loaded MEA (a) and 4A1PPD (b); element mapping images of CS1018 corroded in CO_2-loaded MEA (c, d, e, f) and 4A1PPD (g, h, i., *j*).

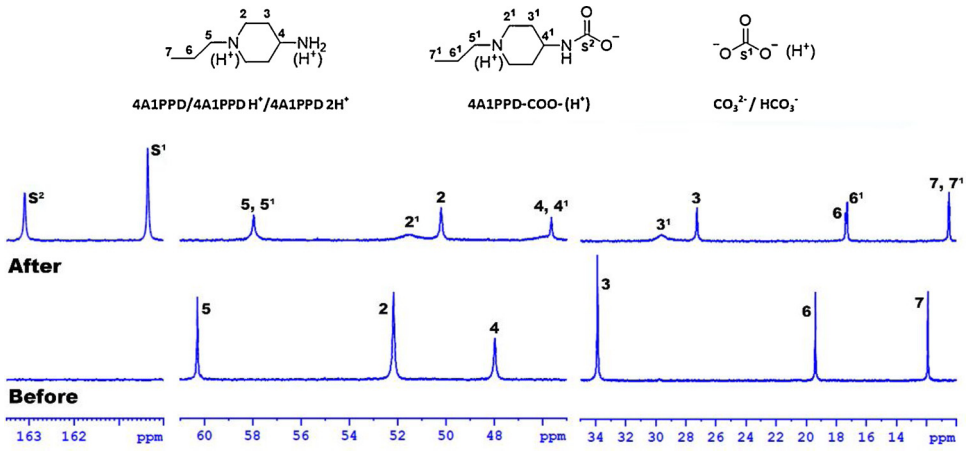

Fig. 6. ^{13}C NMR spectra of 4A1PPD before and after CO_2 loading.

Table 4
Concentration (mol/L) of bicarbonate (C_B) and carbamate (C_C) in amines after CO_2 loading determined from ^{13}C NMR spectra.

Speciation	MEA	1,3-DAP	3MAPA	3DMA1PA	4APD	4A1PPD
C_B	1.83	1.78	1.95	1.98	2.25	2.47
C_C	1.83	1.75	1.72	1.73	1.49	1.71

Table 5
Photographs and mass loss of CS1018 before and after corrosion in CO_2-loaded MEA, 3DMA1PA and 4A1PPD solutions.

Discs	Before	MEA	3DMA1PA	4A1PPD
Photographs				
Mass loss (mg)	0	12.73	3.74	3.17

on the steel surface. The results of mass loss and obtained from ICP-OES further confirm that the 4A1PPD solution has the lowest corrosion.

The crystal structure of the film coated on the surface of the CS1018 discs was determined using XRD. As depicted in Fig. 7a, the characteristic peaks of Fe around 44.8° ((1 1 0) peak), 65.1° ((2 0 0) peak) and 82.4° ((2 1 1) peak) were observed before corrosion (PDF#00-001-1267)(Fortas et al., 2018). The new substances formed on the surface of each disc after hydrothermal corrosion were identified by comparing them with the characteristic patterns of the standard component obtained under the same radiation beam (presented below each diffractogram). New peaks were detected on all samples. On the disc corroded in MEA solution (Fig. 7b), the major component of the film is chukanovite ($Fe_2CO_3(OH)_2$, PDF#00-060-0353); a small quantity of magnetite (Fe_3O_4, PDF#04-012-7038) (Zheng et al., 2016c) was also detected. This result is consistent with previous reports of corrosion scale in MEA solutions (Srinivasan et al., 2013; Zheng et al., 2016c). Peaks characteristic of goethite (α-FeOOH, PDF#01-084-8278) (Bao et al., 2012) and Fe were seen in the diffractogram collected after

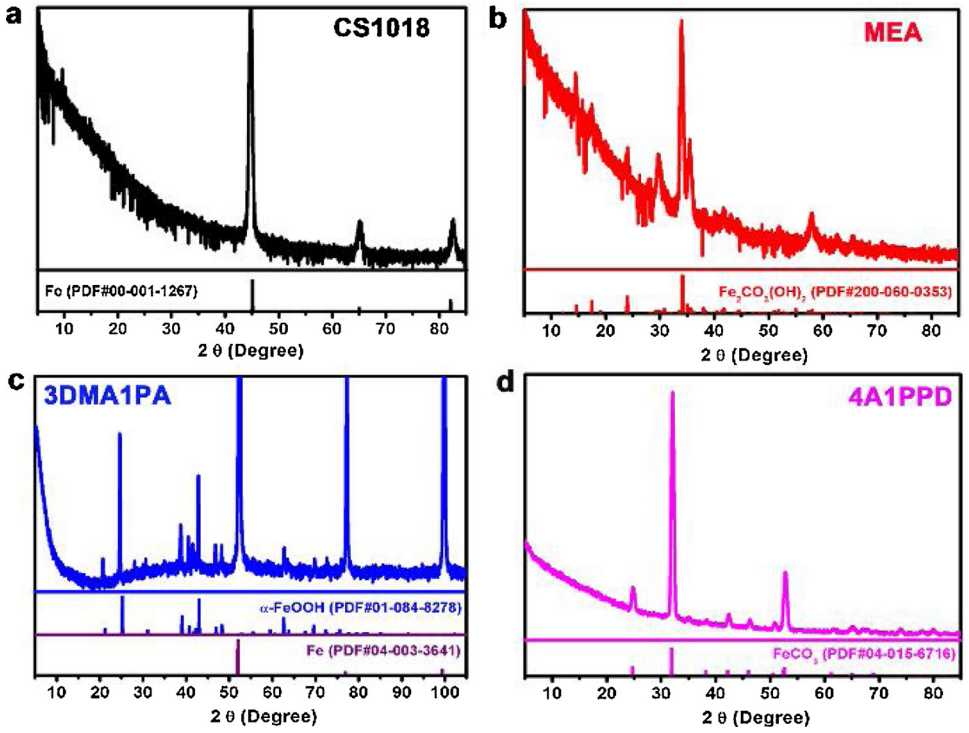

Fig. 7. X-ray diffraction measurements of CS1018 before (a) and after corrosion in CO_2-loaded MEA (b), 3DMA1PA (c) and 4A1PPD (d).

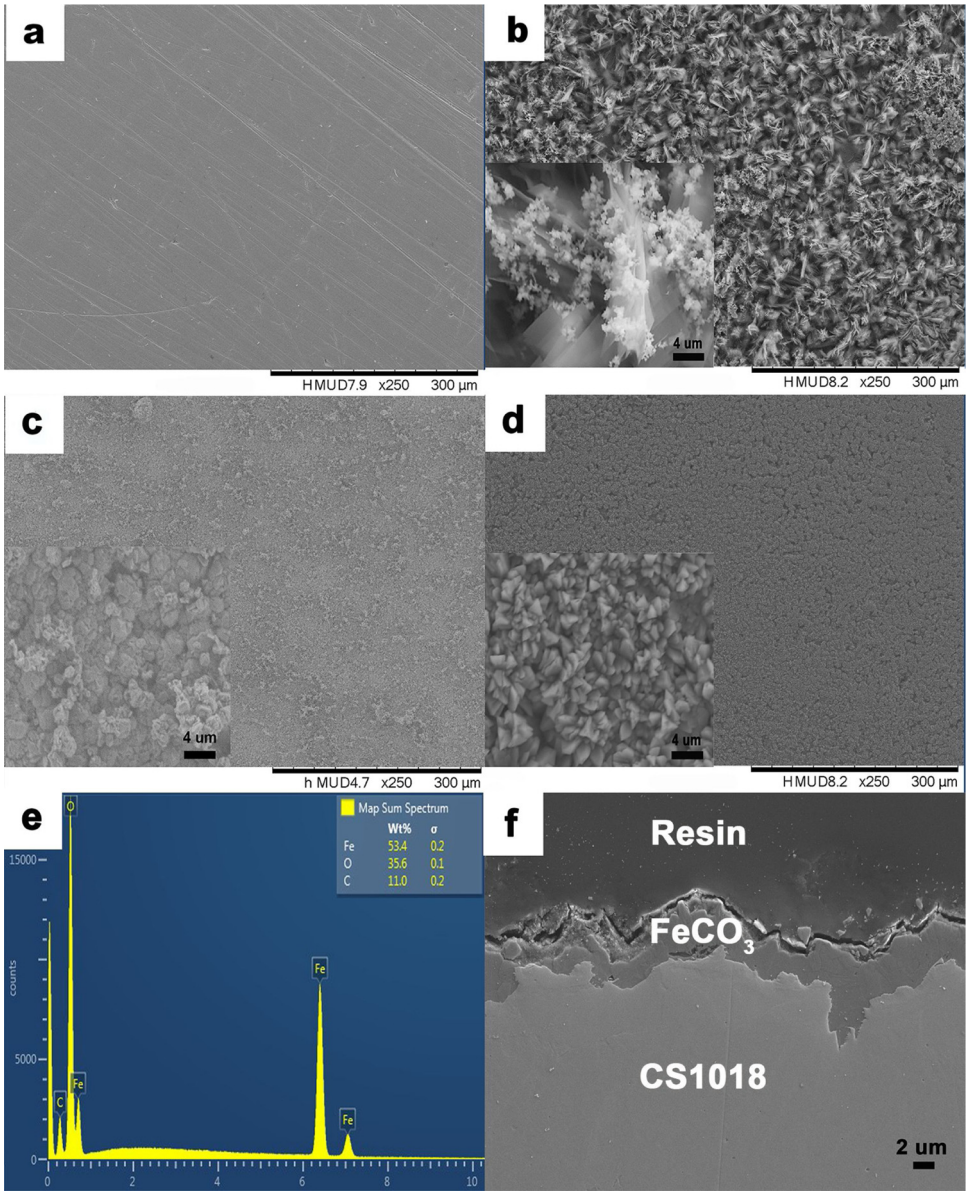

Fig. 8. Scanning electron microscope (SEM) images of CS1018 samples (a) before and after hydrothermal corrosion in CO_2-loaded (b) MEA, (c) 3DMA1PA and (d) 4A1PPD solutions; (e) energy dispersive spectroscopy image; (f) SEM cross-section of CS1018 after treatment in CO_2-loaded 4A1PPD solution.

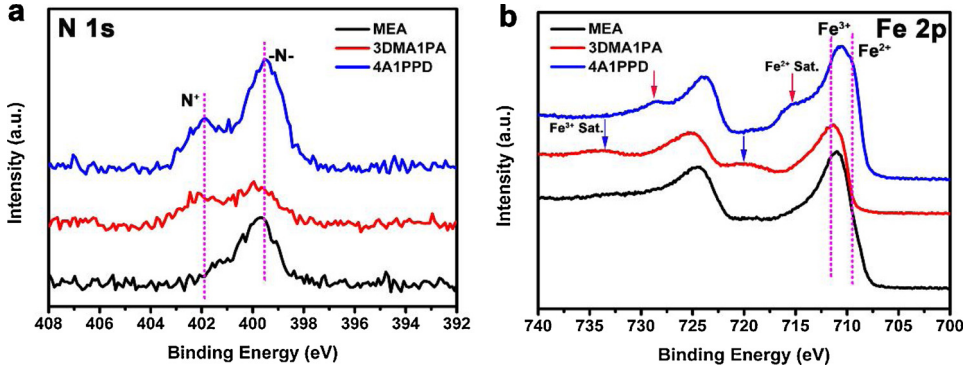

Fig. 9. X-ray photo spectra of samples after hydrothermal corrosion in CO_2-loaded MEA, 3DMA1PA and 4A1PPD solutions; (a) N 1s and (b) Fe 2p spectra.

corrosion in 3DMA1PA solution (Fig. 7c). After the corrosion treatment in 4A1PPD solution (Fig. 7d), a uniform $FeCO_3$ (PDF#04-015-6716) (Zheng et al., 2016c) film was produced, with characteristic XRD peaks located at 24.7, 32.0, 42.3, 46.2, 50.8 and 52.9°. The formation of a dense $FeCO_3$ film such as the one observed in this study is an efficient way to mitigate the corrosion of carbon steel (Emori et al., 2017; Sun et al., 2012; Zheng et al., 2016a).

SEM measurements were also performed to observe the surface

morphologies of CS1018 before (Fig. 8a) and after hydrothermal corrosion treatment in CO_2-loaded MEA (Fig. 8b), 3DMA1PA (Fig. 8c) and 4A1PPD (Fig. 8d) solutions. The initial smooth surface of CS1018 became rougher after corrosion in each solution, illustrating that corrosion occurred and some products formed a film on the metal surface during hydrothermal treatment. After corrosion in MEA solution, the surface of CS1018 was fully coated with nanosheets, and some nanoparticles had grown on the top of the lamellar structure. According to the XRD results and reports in the literature (Zheng et al., 2016a,c), the nanosheets and nanoparticles are $Fe_2CO_3(OH)_2$ and Fe_3O_4, respectively. A 'cotton ball' morphology was observed after corrosion in 3DMA1PA solution, which is similar to the study by Morcillo et al. (de la Fuente et al., 2011). The surface of CS1018 is covered with nano-rhombohedral structures after corrosion in 4A1PPD solution; this morphology is also in agreement with the reported structure of $FeCO_3$ (Sedransk Campbell et al., 2017; Zheng et al., 2016a). These results demonstrate that a denser $FeCO_3$ film is formed on the surface of CS1018 after corrosion in 4A1PPD solution, which demonstrates that a more efficient protective film is produced.

The chemical composition of the surface after hydrothermal corrosion treatment in 4A1PPD solution was analysed using EDS technology. As depicted in Fig. 8e, high levels of the elements C (11 %) and O (35 %) were detected, in addition to Fe. This further supports the formation of a $FeCO_3$ protective film during the hydrothermal corrosion in 4A1PPD solution.

The cross-section of the sample exposed to 4A1PPD solution (Fig. 8f) shows that the film with the thickness of $2-8$ μm is wavy, with thick and thin sections. This is caused by the non-uniform distribution of chemical, and physical factors such as the direction of crystallites and environmental deposits.

The XPS data shown in Fig. 9 provide further interpretation of the corrosion product on the CS1018 surface after hydrothermal corrosion. N 1s high resolution spectra are shown in Fig. 9a. The main peak was observed between 399.5 and 400 eV, a binding energy (BE) typical for amides, and would be consistent with coordinated N on the surface of corroded CS1018. The higher BE around $401.5-402$ eV is assigned to protonated N ($^+$NH-) (Zarrok et al., 2012). The Fe 2p spectra, particularly the $2p_{3/2}$ peak in Fig. 9b, provide some information about different oxidation states of Fe after hydrothermal treatment. Spectral features due to Fe^{2+} (main peak below 710 eV, plus broad satellite peak around 715 eV) and Fe^{3+} (main peak at ca. 711 eV, plus broad satellite peak just below 720 eV) (Biesinger et al., 2011) were observed. The coexistence of Fe^{2+} and Fe^{3+} in the samples further illustrates the formation of Fe_3O_4 film on the surface of CS1018 after corrosion in MEA solution, which is consistent with published literature (Fan et al., 2016; Kim et al., 1997). After hydrothermal corrosion in 3DMA1PA solution, the peaks of $2p_{3/2}$ and $2p_{1/2}$ shifted to a higher BE because of the formation of α-FeOOH, and a satellite peak (Sat.) located around 720.0 eV reveals the existence of Fe^{3+} (Guan et al., 2016). After treatment in 4A1PPD solution, we observed Sat. peaks around 715.0 eV, which is the characteristic peak of Fe^{2+} (McIntyre and Zetaruk, 1977). Combining the results of XRD, SEM and XPS, we conclude that a dense protective $FeCO_3$ film with nano-rhombohedral morphology was formed on the surface of CS1018 after corrosion in 4A1PPD solution.

In this study, we used a short period (nine days) of hydrothermal corrosion to investigate the surface properties of corroded CS1018. We acknowledge that this method may not be effective in determining the longer-term corrosion behaviour and plan to carry out the relevant corrosion experiments to study the process in more detail in subsequent work.

4. Conclusions

The current study focused on the corrosion behaviour of carbon steel in 4A1PPD, with parallel investigation of related diamines to explore the relationship between amine structure and corrosivity to carbon steel under post-combustion CO_2 capture conditions. We found that corrosion rates decreased with a greater number of methyl substituents on the nitrogen atom (i.e. 1° to 2° to 3° amines). Moreover, the corrosion rate decreased when the amine structure changed from linear to cyclic. These structural changes also affected the ratio of bicarbonate to carbamate in solution, which is linked to corrosion rate. 4A1PPD had the lowest corrosion rate in this study, which was approximately half the corrosion rate of the benchmark solvent MEA. Surface analysis confirmed that a dense $FeCO_3$ protective film with nano-rhombohedral morphology was formed on the surface of CS1018 after corrosion in the CO_2-loaded 4A1PPD solution. This work suggests that future development of novel diamines for CO_2 capture should focus on cyclic structures containing tertiary amines, in order to reduce their potential to cause corrosion on carbon steel.

Declaration of Competing Interest

I and other authors declare that we have no any conflict of interests with others.

Acknowledgments

The authors appreciate the technical and scientific support from the Biophysics group of CSIRO Manufacturing in Australia, especially Dr Thomas Gengenbach, Dr Aaron Seeber, Dr Malisja de Vries, Winston Liew and Mark Greaves. The authors would also like to acknowledge the financial support from the National Natural Science Foundation of China (Grant No. 21477084), and also acknowledge the financial support from the China Scholarship Council and CSIRO Energy.

References

Bao, W., Haobin, W., Le, Y., Rong, X., Teik-Thye, L., Wen, L.X., 2012. Template-free formation of uniform urchin-like α-FeOOH hollow spheres with superior capability for water treatment. Adv. Mater. 24, 1111–1116.

Behrens, R., von Harbou, E., Thiel, W.R., Böttinger, W., Ingram, T., Sieder, G., Hasse, H., 2017. Monoalkylcarbonate formation in methyldiethanolamine–H_2O–CO_2. Ind. Eng. Chem. Res. 56, 9006–9015.

Biesinger, M.C., Payne, B.P., Grosvenor, A.P., Lau, L.W.M., Gerson, A.R., Smart, R.S.C., 2011. Resolving surface chemical states in XPS analysis of first row transition metals, oxides and hydroxides: Cr, Mn, Fe, Co and Ni. Appl. Surf. Sci. 257, 2717–2730.

Billingham, M.A., Lee, C.H., Smith, L., Haines, M., James, S.R., Goh, B.K.W., Dvorak, K., Robinson, L., Davis, C.J., Peralta-Solorio, D., 2011. Corrosion and materials selection issues in carbon capture plants. Energy Procedia 4, 2020–2027.

Conway, W., Beyad, Y., Richner, G., Puxty, G., Feron, P., 2015a. Rapid CO_2 absorption into aqueous benzylamine (BZA) solutions and its formulations with monoethanolamine (MEA), and 2-amino-2-methyl-1-propanol (AMP) as components for post combustion capture processes. Chem. Eng. J. 264, 954–961.

Conway, W., Bruggink, S., Beyad, Y., Luo, W., Melián-Cabrera, I., Puxty, G., Feron, P., 2015b. CO_2 absorption into aqueous amine blended solutions containing monoethanolamine (MEA), N,N-dimethylethanolamine (DMEA), N,N-diethylethanolamine (DEEA) and 2-amino-2-methyl-1-propanol (AMP) for post-combustion capture processes. Chem. Eng. Sci. 126, 446–454.

Conway, W., Fernandes, D., Beyad, Y., Burns, R., Lawrance, G., Puxty, G., Maeder, M., 2013. Reactions of CO_2 with aqueous piperazine solutions: formation and decomposition of mono- and dicarbamic acids/carbamates of piperazine at 25.0 degrees C. J. Phys. Chem. A 117, 806–813.

de la Fuente, D., Díaz, I., Simancas, J., Chico, B., Morcillo, M., 2011. Long-term atmospheric corrosion of mild steel. Corros. Sci. 53, 604–617.

Emori, W., Jiang, S.L., Duan, D.L., Ekerenam, O.O., Zheng, Y.G., Okafor, P.C., Qiao, Y.X., 2017. Corrosion behavior of carbon steel in amine-based CO_2 capture system: effect of sodium sulfate and sodium sulfite contaminants. Mater. Corros. 68, 674–682.

Fan, H., Niu, R., Duan, J., Liu, W., Shen, W., 2016. Fe_3O_4@carbon nanosheets for all-solid-state supercapacitor electrodes. ACS Appl. Mater. Inter. 8, 19475–19483.

Fortas, G., Saidoun, I., Abboud, H., Gabouze, N., Haine, N., Manseri, A., Zergoug, M., Menari, H., Sam, S., Cheraga, H., Bozetine, I., 2018. Synthesis of nanocrystalline α-Fe_2O_3 by using thermal oxidation of Fe Films. J. Phys.: Conference Series 987, 012040.

G1, A., 1999. ASTM Standard G1-90 (Reapproved 1999), Standard Practice for Preparing, Cleaning, and Evaluating Corrosion Test Specimens. ASTM, West Conshohocken, PA, pp. 15–21.

Gao, J., Wang, S., Sun, C., Zhao, B., Chen, C., 2012. Corrosion behavior of carbon steel at typical positions of an amine-based CO_2 capture pilot plant. Ind. Eng. Chem. Res. 51, 6714–6721.

Garcia-Arriaga, V., Alvarez-Ramirez, J., Amaya, M., Sosa, E., 2010. H_2S and O_2 influence on the corrosion of carbon steel immersed in a solution containing 3 M

diethanolamine. Corros. Sci. 52, 2268–2279.
Guan, C., Zhao, W., Hu, Y., Ke, Q., Li, X., Zhang, H., Wang, J., 2016. High-performance flexible solid-state Ni/Fe battery consisting of metal oxides coated carbon cloth/carbon nanofiber electrodes. Adv. Energy Mater. 6, 1601034.
Guo, X.P., Tomoe, Y., 1998. Electrochemical behavior of carbon steel in carbon dioxide-saturated diglycolamine solutions. Corros. 54, 931–939.
Hatchell, D., Liu, H., Namjoshi, O., Rochelle, G.T., 2015. Thermal degradation and corrosion of amines for CO_2 capture. Chem. Eng. 679, 8–46.
Kim, Y.J., Gao, Y., Chambers, S.A., 1997. Selective growth and characterization of pure, epitaxial α-Fe_2O_3(0001) and Fe_3O_4(001) films by plasma-assisted molecular beam epitaxy. Surf. Sci. 371, 358–370.
Kladkaew, N., Idem, R., Tontiwachwuthikul, P., Saiwan, C., 2009. Corrosion behavior of carbon steel in the monoethanolamine $-H_2O-CO_2-O_2-SO_2$ system. Ind. Eng. Chem. Res. 48, 8913–8919.
Krzemień, A., Więckol-Ryk, A., Smoliński, A., Koteras, A., Więcław-Solny, L., 2016. Assessing the risk of corrosion in amine-based CO_2 capture process. J. Loss Prev. Process Ind. 43, 189–197.
Lebrini, M., Lagrenée, M., Vezin, H., Traisnel, M., Bentiss, F., 2007. Experimental and theoretical study for corrosion inhibition of mild steel in normal hydrochloric acid solution by some new macrocyclic polyether compounds. Corros. Sci. 49, 2254–2269.
Li, L., Burns, R.C., Maeder, M., Puxty, G., Wang, S., Yu, H., 2017. The determination of the Henry's Coefficient of reactive gases - an example of CO_2 in aqueous solutions of monoethanolamine (MEA). Chem. Eng. Sci. 173, 474–482.
Li, X., Deng, S., Fu, H., 2011. Synergistic inhibition effect of 6-benzylaminopurine and iodide ion on the corrosion of cold rolled steel in H_3PO_4 solution. Corros. Sci. 53, 3704–3711.
Li, X.Q., Yang, Q., Pearson, P., Yu, B., Puxty, G., Xiao, D., 2018. The application of trans-1,4-diaminocyclohexane as a bicarbonate formation rate promoter in CO_2 capture. Fuel 226, 479–489.
McIntyre, N.S., Zetaruk, D.G., 1977. X-ray photoelectron spectroscopic studies of iron oxides. Anal. Chem. 49, 1521–1529.
Nainar, M., Veawab, A., 2009. Corrosion in CO_2 capture process using blended monoethanolamine and piperazine. Ind. Eng. Chem. Res. 48, 9299–9306.
Nešić, S., Lee, K.-L.J., 2003. A mechanistic model for carbon dioxide corrosion of mild steel in the presence of protective iron carbonate films—part 3: film growth model. Corros. 59, 616–628.
Nielsen, A.L.K.R., 1997. Gas Purification, 5th edition. Gulf Professional Publishing.
Pearson, P., Hollenkamp, A.F., Meuleman, E., 2013. Electrochemical investigation of corrosion in CO_2 capture plants—influence of amines. Electrochim. Acta 110, 511–516.
Raeissi, K., Golozar, M.A., 2009. Passivation behavior of carbon steel in hydrogen sulfide-containing diethanolamine and diglycolamine solutions. Corros. 65, 595–600.
Rochelle, G.T., 2012. Thermal degradation of amines for CO_2 capture. Current pinion in Chemical Engineering 1, 183–190.
Sedransk Campbell, K.L., Yu, L.C.Y., Williams, D.R., 2017. Siderite corrosion protection for carbon steel infrastructure in post-combustion capture plants. Inter. J. Greenh. Gas Con. 58, 232–245.
Sığırcık, G., Tüken, T., Erbil, M., 2016. Assessment of the inhibition efficiency of 3,4-diaminobenzonitrile against the corrosion of steel. Corros. Sci. 102, 437–445.
Soosaiprakasam, I.R., Veawab, A., 2008. Corrosion and polarization behavior of carbon steel in MEA-based CO2 capture process. Inter. J. Greenh. Gas Con. 2, 553–562.
Srinivasan, S., Veawab, A., Aroonwilas, A., 2013. Low Toxic Corrosion inhibitors for amine-based CO_2 capture process. Energy Procedia 37, 890–895.
Sun, J.B., Zhang, G.A., Liu, W., Lu, M.X., 2012. The formation mechanism of corrosion scale and electrochemical characteristic of low alloy steel in carbon dioxide-saturated solution. Corros. Sci. 57, 131–138.
Sun, W., Nesic, S., 2006. Basics revisited: kinetics of iron carbonate scale precipitationin CO_2 corrosion. Corrosion paper no. 06365, 1–21.
Tang, Y., Yang, X., Yang, W., Wan, R., Chen, Y., Yin, X., 2010. A preliminary investigation of corrosion inhibition of mild steel in 0.5M H_2SO_4 by 2-amino-5-(n-pyridyl)-1,3,4-thiadiazole: polarization, EIS and molecular dynamics simulations. Corros. Sci. 52, 1801–1808.
Tomoe, Y., Shimizu, M., Kaneta, H., 1996. Active Dissolution and Natural Passivation of Carbon Steel in Carbon Dioxide-loaded Alkanolamine Solutions. NACE International, Houston, TX (United States).
Veawab, A., Aroonwilas, A., 2002. Identification of oxidizing agents in aqueous amine–CO_2 systems using a mechanistic corrosion model. Corros. Sci. 44, 967–987.
Xiao, M., Cui, D., Yang, Q., Liang, Z., Puxty, G., Conway, W., Feron, P., 2019. Advanced designer amines for CO_2 capture: interrogating speciation and physical properties. Inter. J. Greenh. Gas Con. 82, 8–18.
Yang, Q., Puxty, G., James, S., Bown, M., Feron, P., Conway, W., 2016. Toward intelligent CO_2 capture solvent design through experimental solvent development and amine synthesis. Energy Fuels 30, 7503–7510.
Zarrok, H., Zarrouk, A., Hammouti, B., Salghi, R., Jama, C., Bentiss, F., 2012. Corrosion control of carbon steel in phosphoric acid by purpald – weight loss, electrochemical and XPS studies. Corros. Sci. 64, 243–252.
Zheng, L., Landon, J., Koebcke, N.C., Chandan, P., Liu, K., 2015. Suitability and stability of 2-mercaptobenzimidazole as a corrosion inhibitor in a post-combustion CO_2 capture system. Corros. 71, 692–702.
Zheng, L., Landon, J., Matin, N.S., Liu, K., 2016a. $FeCO_3$ Coating process toward the corrosion protection of carbon steel in a postcombustion CO_2 capture system. Ind. Eng. Chem. Res. 55, 3939–3948.
Zheng, L., Landon, J., Matin, N.S., Thomas, G.A., Liu, K., 2016b. Corrosion mitigation via a pH stabilization method in monoethanolamine-based solutions for post-combustion CO_2 capture. Corros. Sci. 106, 281–292.
Zheng, L., Landon, J., Zou, W., Liu, K., 2014. Corrosion benefits of piperazine as an alternative CO_2 capture solvent. Ind. Eng. Chem. Res. 53, 11740–11746.
Zheng, L., Matin, N.S., Landon, J., Thomas, G.A., Liu, K., 2016c. CO_2 loading-dependent corrosion of carbon steel and formation of corrosion products in anoxic 30 wt.% monoethanolamine-based solutions. Corros. Sci. 102, 44–54.